Journal of Dental Sciences 20 (2025) 2353–2362

Available online at www.sciencedirect.com

ScienceDirect

journal homepage: www.e-jds.com

Original Article

Beyond dental radiographs, a radiomics-based study for the classification of caries extension and depth

Niccolò Giuseppe Armogida [a†], Francesca Angelone [b*†], Parisa Soltani [a], Luigi Esposito [a], Mario Sansone [b], Sandro Rengo [a], Francesco Amato [b], Carlo Rengo [a], Gianrico Spagnuolo [a,c**], Alfonso Maria Ponsiglione [b]

[a] *Department of Neurosciences, Reproductive and Odontostomatological Sciences, University of Naples 'Federico II', Naples, Italy*
[b] *Department of Electrical Engineering and Information Technology, University of Naples 'Federico II', Naples, Italy*
[c] *School of Dentistry, College of Dental Medicine, Kaohsiung Medical University, Kaohsiung, Taiwan*

Received 30 March 2025; Final revision received 6 April 2025
Available online 16 April 2025

KEYWORDS
Machine learning;
Radiomics;
Dental caries;
Dental photography

Abstract *Background/purpose:* Traditional caries detection relies on visual and radiographic analysis. While deep learning has been applied to classify caries extent, no studies classify caries depth using radiomic features in intraoral photographic images. This study evaluated a radiomics-based approach with machine learning (ML) to classify caries extent and depth, traditionally assessed via radiographs, using intraoral photographs.
Materials and methods: Standardized intraoral photographs were taken with a Nikon D7500 and Macro Flash MF-R76. Only images of healthy teeth or carious lesions were included. Images were resized, segmented with Labelme, and classified using ICDAS and E-D scales. Data augmentation increased sample size. Radiomic features were extracted for each color channel using Pyradiomics. Feature selection methods (AUC-ROC, ReliefF, LASSO, backward selection) were applied within 5-fold cross-validation to prevent bias. ML classifiers (LDA, k-NN, SVM, NNET) evaluated accuracy, sensitivity, and specificity. Model explainability assessed feature influence via partial dependence plots, residual analysis, and break–down profile.
Results: NNET with backward selection achieved high accuracy (87.6%–95.4%). Sensitivity and specificity ranged from 61.5% to 93% and 73%–90%, respectively. Green and red channels

* Corresponding author. Department of Electrical Engineering and Information Technology, University of Naples 'Federico II', Via Claudio, 21, Naples, 80125, Italy.
** Corresponding author. Department of Neurosciences, Reproductive and Odontostomatological Sciences, University of Naples 'Federico II', Via Sergio Pansisi 5, Naples, 80131, Italy.
E-mail addresses: francesca.angelone@unina.it (F. Angelone), gspagnuo@unina.it (G. Spagnuolo).
† These authors contributed equally to this work.

https://doi.org/10.1016/j.jds.2025.04.006

significantly impacted predictions, with texture features being critical. The red channel's greater impact reflects its ability to mimic near-infrared light transillumination, enhancing contrast between healthy and decayed tissue. The blue channel had lesser influence, but combined RGB channels yielded the best accuracy.
Conclusion: Radiomics enables caries depth classification from intraoral photographs, offering a non-invasive, cost-effective alternative to radiographs. This approach could revolutionize diagnostics by reducing reliance on invasive radiological techniques, using accessible and affordable equipment.

Introduction

Machine learning (ML) is increasingly applied in dentistry, particularly in orthodontic analysis,[1] periodontal disease assessment,[2] head and neck cancer detection,[3] and radiographic artifact management.[4] ML has shown promising results in dental caries detection,[5] offering objective, accurate, and efficient support while enabling innovative clinical approaches.

Traditional caries detection relies on visual examination and radiographic analysis.[6,7] However, high-resolution intraoral photographic imaging is now commonly used for diagnosis and treatment monitoring. Artificial intelligence (AI), particularly deep learning (DL), enhances caries detection in such images,[8] identifying early-stage lesions like white spots and surface demineralization, thereby facilitating early intervention and prevention.

Radiomics, widely used in medical imaging, extracts quantitative features related to texture, shape, and intensity, offering insights beyond human perception.[9–15] By converting medical images into high-dimensional data, radiomics aids disease characterization, prognosis, and treatment planning. Its integration with ML enables correlation identification between extracted features and clinical outcomes, advancing precision medicine.[16] In dentistry, initial studies suggest radiomics-based diagnostic accuracy comparable to that of professionals.[17–19] However, its application in intraoral photographic analysis remains underexplored.

A breakthrough in dental healthcare could arise from leveraging AI to extract diagnostic information from digital photographs. This approach may enhance diagnostic efficiency, improve patient outcomes, and reduce reliance on radiological methods. Additionally, it could ensure the use of simple, affordable and technologically less complex devices,[20] fostering the growth of digital dentistry and reaching even more disadvantaged regions. Compared to the wide range of complex and computationally demanding deep-learning architecture for dental image segmentation and recognition, the potential offered by radiomics and machine learning in intraoral diagnostics from photographs is still poorly explored.

This study highlighted AI's role in advancing non-invasive, high-precision dental diagnostics by demonstrating how radiomics and ML could extract diagnostic insights from intraoral photographs. Therefore, the aim of the study was multiple: (i) to evaluate the potential of radiomics and machine learning in dental diagnostics, with particular reference to caries classification; (ii) to demonstrate the feasibility of predicting caries depth directly from RGB images, without having to resort to X-ray images; (iii) to explain the clinical - physiological significance of the most predictive radiomic characteristics.

Materials and methods

The methodological workflow followed in this study is represented in Fig. 1.

Imaging data

This is a retrospective study. Images were acquired using a Nikon D7500 SLR camera with a Nikon Micro 105 mm lens (Nikon Corporation, Tokyo, Japan) and Macro Flash MF-R76 illumination (Neewer, Shenzhen, China). Before imaging, teeth were thoroughly cleaned and dried to ensure optimal visibility of caries lesions. Posterior teeth were imaged indirectly using intraoral mirrors (Reflect-Rhod; Hager & Werken, Duisburg, Germany), which were preheated to prevent condensation on the mirror surface during photography. Each image was captured at a resolution of 150 dpi with a color depth of 24 bits. Images were recorded in the sRGB color space, ensuring consistent color representation and facilitating accurate analysis of caries lesions. Bitewing radiographs were collected for each image in the dataset to assess and classify caries depth.

Data pre-processing and segmentation

Images were cropped, resized to 512 × 512 pixels, and carious lesions were manually segmented using Labelme tool (MIT Computer Science and Artificial Intelligence Laboratory, Cambridge, MA, USA),[21] by two expert calibrated dentists, professors of restorative dentistry and *active members* of the Italian Society of Restorative Dentistry (SIDOC). Any disagreement was resolved through consensus with a third dentist. Subsequently, the segmented regions of interest (ROIs) were labeled according to the International Caries Detection and Assessment System (ICDAS) scale,[22] to evaluate the extension of the carious lesion, and according to the E-D scale to evaluate the depth of the carious lesion, making appropriate comparisons with the respective radiological images available to dentists.

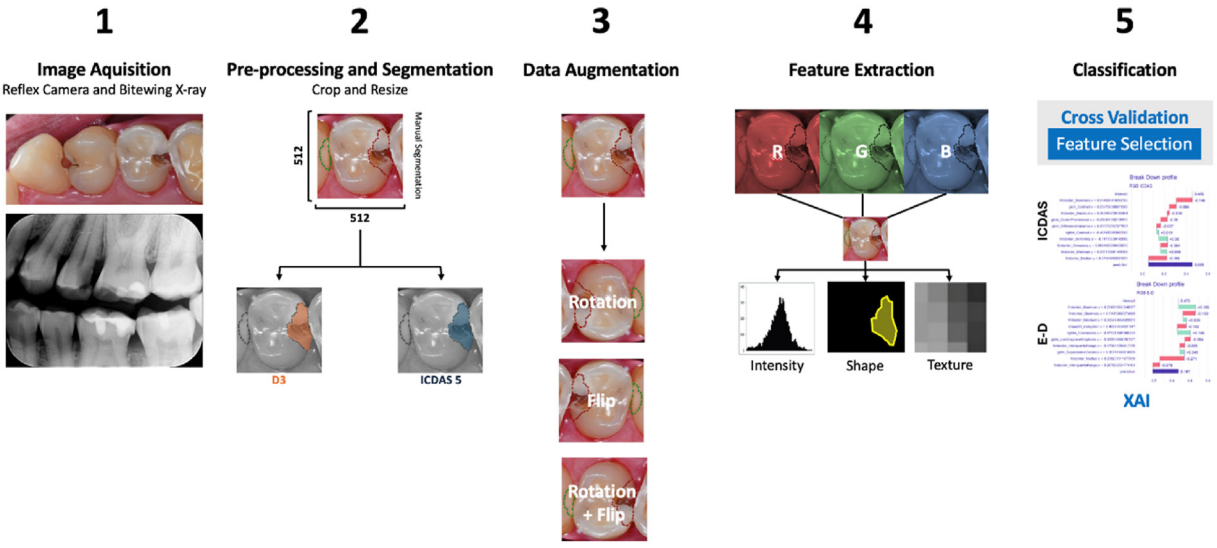

Figure 1 Methodological workflow.

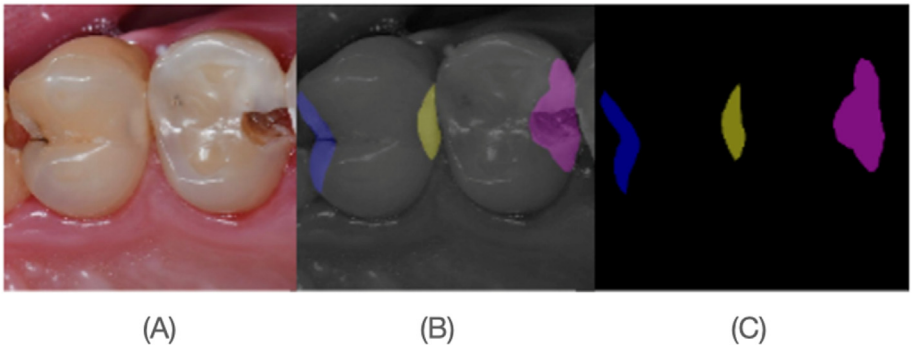

Figure 2 Example of segmented images using Labelme tool. (A) Original cropped and resized image. (B) JPEG class label visualization. (C) Label PNG file (mask).

Segmentations have been exported from Labelme in JSON format and then converted into Pascal Visual Object Classes (VOC) to obtain a label PNG file with the segmented area, as represented in Fig. 2.

Data augmentation

Data augmentation was used to increase the sample size and balance the classes. Specifically, each image was rotated 90, 180, and 270° and flipped vertically and horizontally. It was then rotated and flipped simultaneously. Therefore, the dataset was increased by randomly selecting a balanced number of images in the augmented dataset belonging to each class that could balance the number of original images for each class. A total of 286 occlusal pictures of caries are obtained after data augmentation. Detailed information on the sample size are reported in Figures S1–S4 of Supplementary Materials.

Radiomic features

Per each image, 102 radiomic features were extracted for each of the three color channels (red (R), green (G), and blue (B)) using Pyradiomics,[23] an IBSI compliant software package in Python.[24] The extracted feature classes could be summarized as follows: first order (18 features), shape 2D (9 features), gray level co-occurrence matrix (24 features), gray level run length matrix (16 features), gray level size zone matrix (16 features), neighbouring gray tone difference matrix (5 features), gray level dependence matrix (14 features). Therefore, a total of 306 features were available per image.

Features selection

To ensure that the resulting classification model is unbiased and generalizable to new data, the process of feature selection was included in the cross-validation.[25,26] The most "important" radiomic features for each classifier, i.e. strongly associated with ICDAS and E-D classes, were evaluated using four commonly used algorithms: AUC-ROC analysis.[27,28] ReliefF,[27,29] LASSO,[27,30] and backward selection.[27]

As mentioned, to avoid bias in feature selection, the training set was divided into k = 5 folds of approximately equal size; the selection of the features and the subsequent

classification took place on 4 folds while the performance evaluation was carried out on the held-out fold. A total of 25 features were used for training.

Classification and performance evaluation

An automatic classification between non-severe and severe carious lesions (ICDAS 3,4 VS ICDAS 5,6) and between deep and non-deep lesions (E1, E2, D1 VS D2, D3), whose distribution is reported in Fig. 2, was made using ML algorithms. Four classifiers have been used: linear discriminant analysis (LDA), k-nearest neighbours (k-NN), support vector machine (SVM) and neural networks (NNET).

To evaluate the performance, a 5-fold cross-validation with 100 repetitions was used, training and testing the data on the same sets of randomly chosen preliminary folds taking into account the data leakage due to data augmentation, to make appropriate comparisons.

Table 1 Accuracy, sensitivity and specificity of classification on ICDAS classes.

		NNET			SVM			KNN			LDA		
		Acc	Sens	Spec	Acc	Sens	Spec	Acc	Sens	Spec	Acc	Sens	Spec
Red	Backward	**0.92**	0.92	0.92	**0.92**	0.91	0.91	0.91	0.91	0.91	0.91	0.91	0.91
	Relief	**0.92**	0.92	0.92	0.91	0.90	0.90	**0.92**	0.92	0.92	0.91	0.90	0.90
	LASSO	0.93	0.93	0.93	**0.94**	0.93	0.93	0.92	0.91	0.91	0.93	0.93	0.93
	AUC	**0.92**	0.93	0.93	**0.92**	0.92	0.92	**0.92**	0.92	0.92	0.91	0.92	0.92
Green	Backward	**0.93**	0.92	0.92	0.92	0.91	0.91	0.91	0.91	0.91	0.91	0.89	0.89
	Relief	0.92	0.92	0.92	0.92	0.91	0.91	0.91	0.90	0.90	**0.93**	0.89	0.89
	LASSO	**0.94**	0.92	0.92	0.93	0.92	0.92	0.93	0.91	0.91	0.91	0.92	0.92
	AUC	**0.93**	0.93	0.93	0.92	0.91	0.91	0.92	0.90	0.91	0.90	0.90	0.90
Blue	Backward	**0.93**	0.91	0.91	0.92	0.91	0.91	0.92	0.90	0.90	0.90	0.89	0.89
	Relief	**0.93**	0.91	0.91	0.92	0.91	0.91	0.92	0.89	0.89	**0.94**	0.89	0.89
	LASSO	**0.94**	0.92	0.92	0.93	0.92	0.92	0.93	0.91	0.91	0.91	0.92	0.92
	AUC	**0.92**	0.91	0.91	0.92	0.91	0.91	0.92	0.90	0.90	0.92	0.89	0.89
RGB	Backward	**0.92**	0.92	0.92	0.92	0.91	0.94	0.92	0.91	0.93	0.92	0.90	0.93
	Relief	**0.92**	0.91	0.93	0.92	0.91	0.93	0.91	0.91	0.92	0.92	0.91	0.93
	LASSO	**0.93**	0.92	0.93	**0.93**	0.93	0.94	**0.93**	0.92	0.94	**0.93**	0.93	0.93
	AUC	**0.92**	0.93	0.92	**0.92**	0.92	0.93	0.91	0.91	0.92	0.91	0.90	0.91

Abbreviations: Acc, accuracy; Sens, sensitivity; Spec, specificity; ICDAS, International Caries Detection and Assessment System; NNET, neural network; SVM, support vector machine; KNN, k-nearest neighbor; LDA, linear discriminant analysis; AUC, area under the curve; LASSO, least absolute shrinkage and selection operator; Backward, backward feature elimination; Relief, relevance evaluation using ReliefF algorithm.

Table 2 Accuracy, sensitivity and specificity of classification on E-D classes.

		NNET			SVM			KNN			LDA		
		Acc	Sens	Spec	Acc	Sens	Spec	Acc	Sens	Spec	Acc	Sens	Spec
Red	Backward	**0.93**	0.92	0.92	0.91	0.89	0.89	0.91	0.91	0.91	0.91	0.89	0.89
	Relief	**0.92**	0.92	0.92	0.92	0.89	0.89	0.92	0.91	0.91	0.90	0.89	0.89
	LASSO	0.93	0.92	0.92	0.93	0.92	0.92	0.92	0.90	0.90	**0.94**	0.92	0.92
	AUC	**0.93**	0.92	0.92	**0.93**	0.91	0.91	0.92	0.92	0.92	0.92	0.91	0.91
Green	Backward	**0.92**	0.90	0.90	0.91	0.88	0.88	0.91	0.89	0.89	0.89	0.87	0.87
	Relief	**0.92**	0.90	0.90	0.91	0.89	0.89	0.91	0.88	0.88	0.89	0.86	0.86
	LASSO	0.91	0.89	0.89	0.88	0.86	0.86	**0.92**	0.88	0.88	0.89	0.89	0.89
	AUC	**0.92**	0.91	0.91	0.92	0.90	0.90	0.90	0.87	0.87	0.88	0.87	0.87
Blue	Backward	**0.92**	0.89	0.89	0.92	0.88	0.88	0.91	0.86	0.86	0.91	0.88	0.88
	Relief	**0.92**	0.89	0.89	0.92	0.88	0.88	0.91	0.86	0.86	0.91	0.87	0.87
	LASSO	**0.92**	0.88	0.88	0.91	0.87	0.87	0.92	0.89	0.89	0.88	0.88	0.88
	AUC	**0.92**	0.88	0.88	0.91	0.87	0.87	0.90	0.87	0.87	0.90	0.87	0.87
RGB	Backward	**0.93**	0.92	0.94	0.92	0.90	0.94	0.92	0.90	0.94	0.90	0.88	0.93
	Relief	**0.93**	0.92	0.94	0.92	0.90	0.94	0.92	0.90	0.93	0.90	0.87	0.93
	LASSO	**0.93**	0.91	0.94	**0.93**	0.91	0.95	0.91	0.89	0.94	**0.93**	0.92	0.94
	AUC	**0.93**	0.92	0.94	**0.93**	0.91	0.95	0.92	0.91	0.93	0.91	0.89	0.94

Abbreviations: Acc, accuracy; Sens, sensitivity; Spec, specificity; E-D, Enamel-Dentine scale; NNET, neural network; SVM, support vector machine; KNN, k-nearest neighbor; LDA, linear discriminant analysis; AUC, area under the curve; LASSO, least absolute shrinkage and selection operator; Backward, backward feature elimination; Relief, relevance evaluation using ReliefF algorithm.

The metrics used to evaluate the classification performance were accuracy, sensitivity, and specificity. All analyses were performed in R, using the CARET package.[31]

Explainable AI

Explainability in ML is becoming increasingly important to help extract insights into how these algorithms behave and why one prediction is being made.[32] Partial dependence plots (PDPs)[33] have been explored to show the marginal effect a feature has on the predicted outcome of an ML model. An analysis of the residuals of the predicted value versus the actual values was also done which can help identify where the models deviate in their predictive accuracy. Moving on to local explanations, a Break Down method was applied.[34] All these analyses were performed in R, using the DALEX package.[35]

Results

Tables 1 and 2 show the results for the accuracy, sensitivity, and specificity of the tested models for the ICDAS and E-D classes classification, respectively.

Based on the results obtained from testing the ML models with the different feature selection methods, a non-significant difference can be seen between the

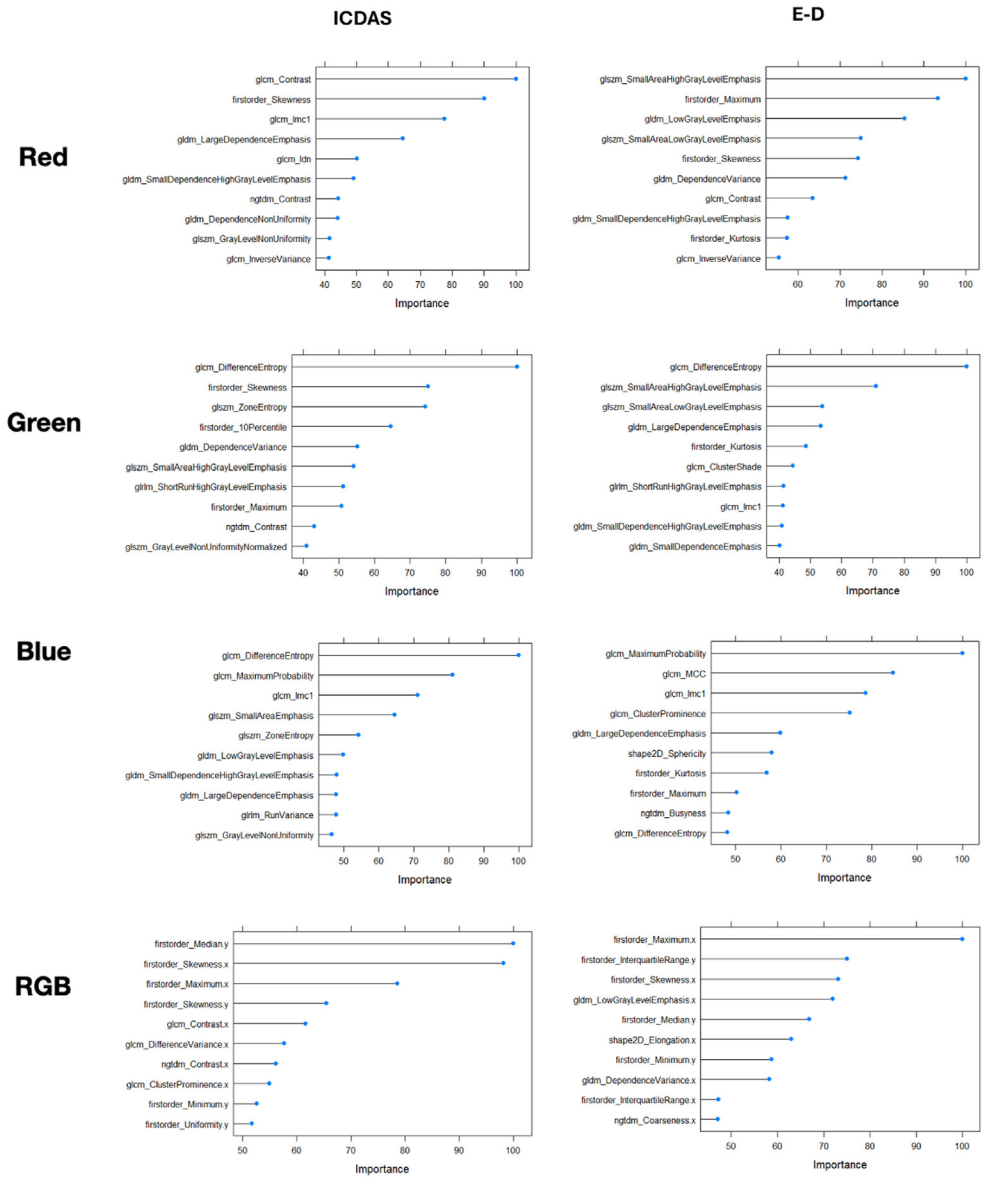

Figure 3 Feature importance analysis for each color channel for ICDAS and E-D classes. For RGB color channels, the features are followed by x when they refer to the red channel and y when they refer to the green channel. Abbreviations: ICDAS, International Caries Detection and Assessment System; E-D, Enamel-Dentine scale; RGB, red green blue; GLCM, gray level co-occurrence matrix; GLSZM, gray level size zone matrix; NGTDM, neighbouring gray tone difference matrix; GLDM, gray level dependence matrix; GLRLM, gray level run length matrix.

different color channels and the different models and feature selection methods. However, the NNET model with the Backward selection method offers comparable results in assessing the depth and extent of caries, therefore it was selected for further investigation into the explainability of this model.

First, the impact of the color channels on the model's prediction was evaluated by defining the most important features of the model, shown in Fig. 3.

Once the most important features for each channel were taken, the PDPs could be visualized to show how these features influence the model's prediction. Fig. 4 shows the first most important feature of each color channel.

A residual analysis was then carried out. Fig. 5 shows the reverse cumulative distribution curves of absolute residuals for the ICDAS and ED classifications. Boxplots of absolute residues are shown in Fig. S5 of Supplementary Materials.

As shown in Fig. 5, considering all the color channels, the absolute residuals are around the value 1 for almost all percentiles. A case-wise analysis was therefore conducted considering the RGB case, applying the Break Down method for the local explanations, as shown in Fig. 6.

Discussion

This study aims to classify dental caries' depth and extension on a set of intraoral photographic images, grouped by ICDAS and E-D classifications. Results show high model performance, with accuracy ranging from 88% to 94% and sensitivity and specificity reaching up to 95% (as from Tables 1 and 2), without significant variability between the different color channels.

This is a particularly interesting result, especially for depth classification on the E-D scale that can be observed in clinical practice only from radiographs. Based on our knowledge, these findings represent a relevant step in moving towards RX-free based caries classification. Indeed,

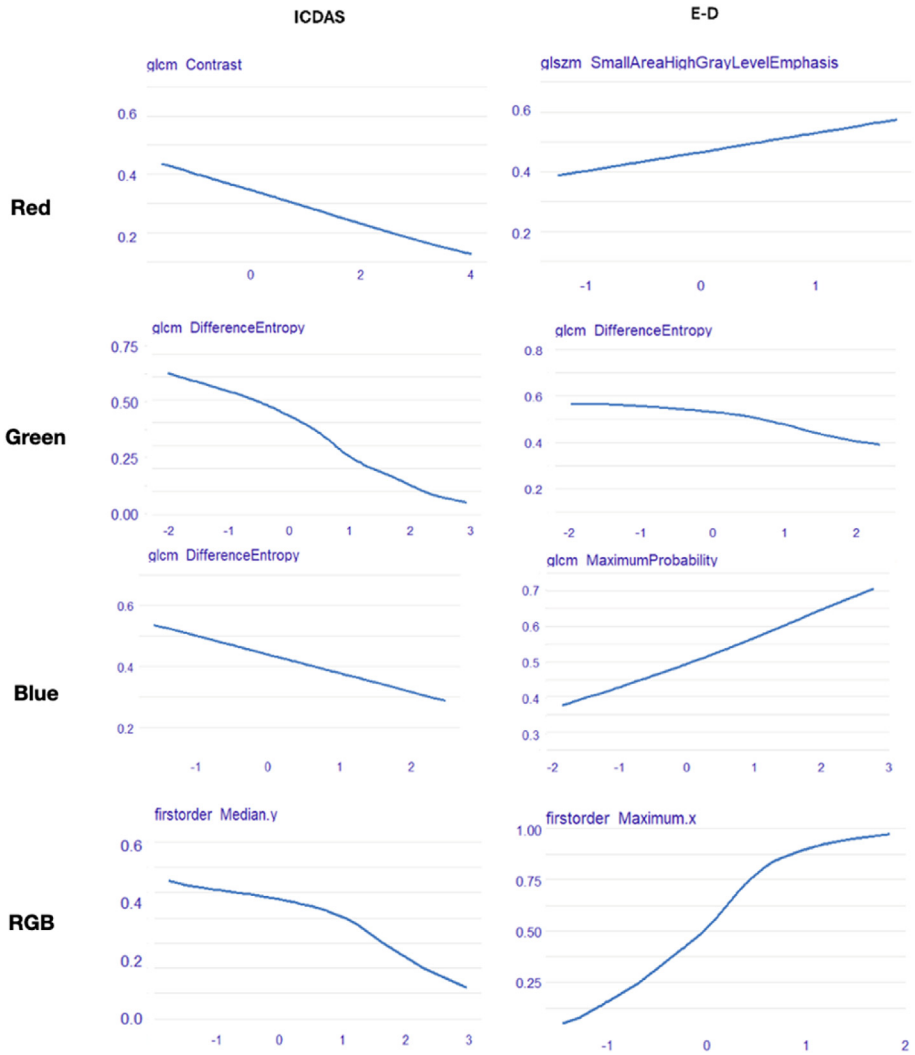

Figure 4 Partial dependence plots for the most important feature for each color channel and the ICDAS and E-D classes. For RGB color channels the features are followed by x when they refer to the red channel and y when they refer to the green channel. Abbreviations: ICDAS, International Caries Detection and Assessment System; E-D, Enamel-Dentine scale; RGB, red green blue; GLCM, Gray level co-occurrence matrix; GLSZM, Gray level size zone matrix.

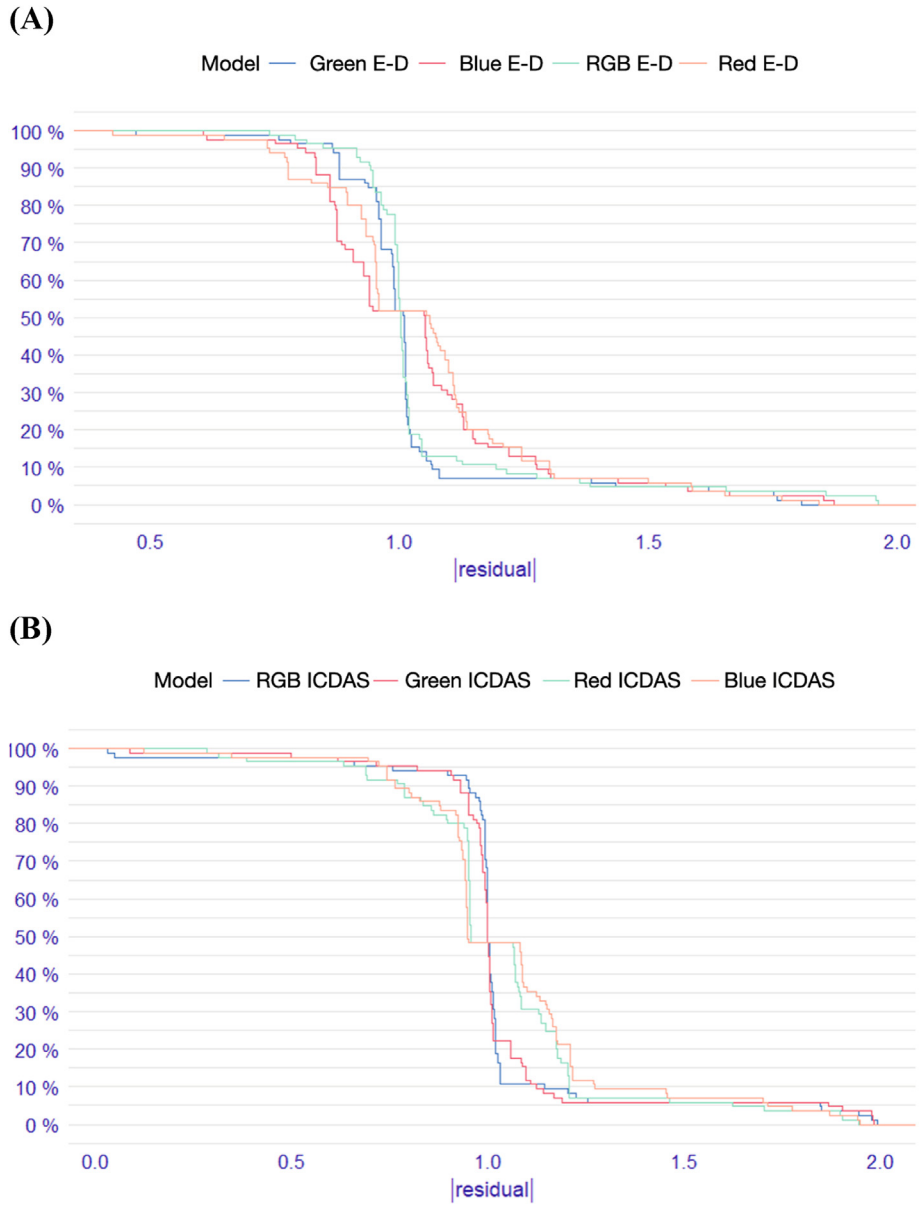

Figure 5 Reverse cumulative distribution curves of absolute residuals (A) for E-D classes and (B) for ICDAS classes. Abbreviations: ICDAS, International Caries Detection and Assessment System; E-D, Enamel-Dentine scale; RGB, red green blue.

they confirm the promising role of radiomics in classifying caries depth starting from intraoral photographic images, thus paving the way to a new paradigm in intraoral diagnostics, which could be mostly based on photographic images without resorting to more invasive radiological methods.

In this field, literature reports accuracy scores for caries extension ranging from 71% to 96% for intraoral photographs, 82%–99.2% for periapical radiographs, and 87.6%–95.4% for bitewing radiographs. Sensitivity and specificity for intraoral pictures range from 73% to 90% and 61.5%–93%, respectively.[6,8] Therefore, despite a small sample, the results of the present study are comparable with the best scores obtained in other studies.

To make the proposed application more trustworthy and clinically significant, this work also explores the potential of explainable AI algorithms to achieve more interpretable and informed decisions. Having chosen the NNET model with backward feature selection as optimal classification approach (accuracy ranging from 92% to 93%), the most important radiomics features have been listed (as from Fig. 3) and analyzed through PDPs to investigate their specific influence on the final model decision.

The red channel's contrast (GLCM texture feature class), which measures local intensity variation (higher values indicating greater differences in neighboring pixel intensities), plays a key role in the ICDAS classification as an increase in contrast shifts the prediction towards class 0 (i.e., less severe caries: ICDAS 2–3). This can be due to the fact that moving towards higher wavelength, as it occurs in near-infrared transillumination, can improve the capability to distinguish carious from healthy tissues thanks to contrast

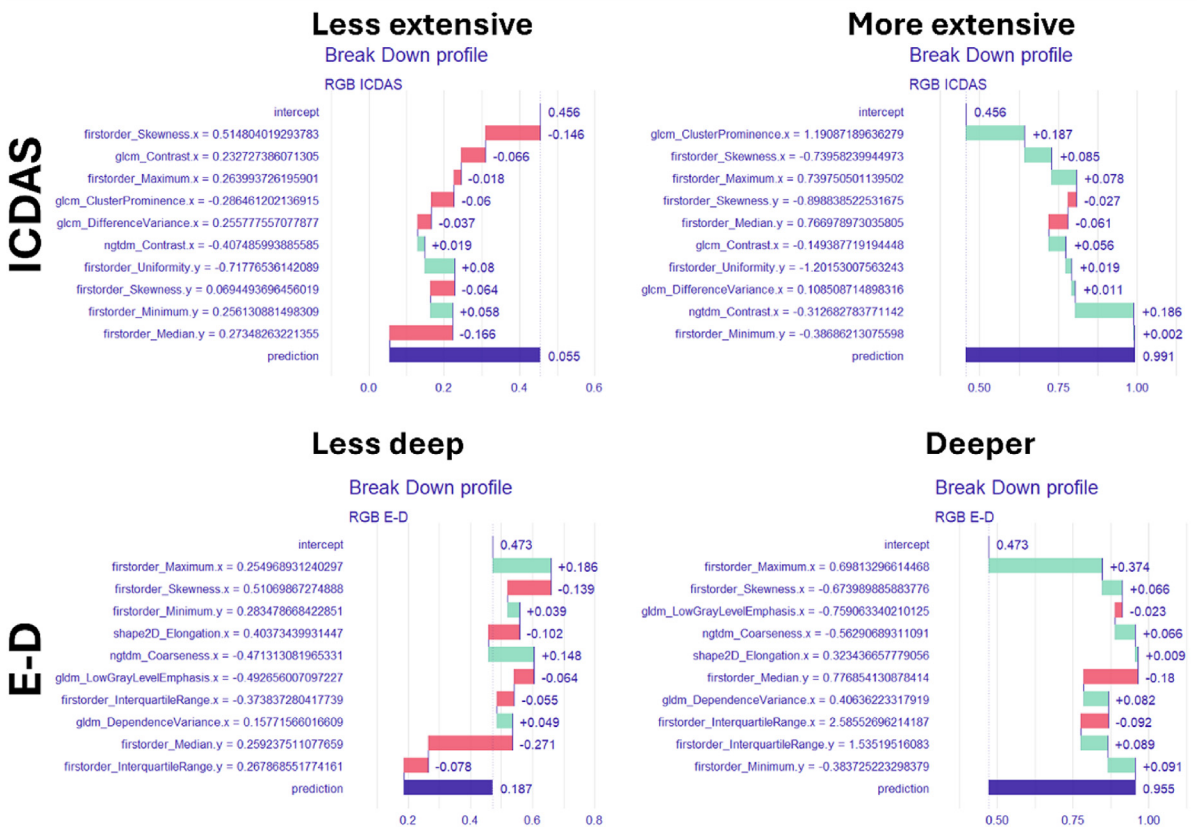

Figure 6 Local explanations for a single observation of class 0 (less extensive or less deep) and 1 (more extensive or deeper) using Break Down profiles. For RGB color channels the features are followed by x, when they refer to the red channel, and y when they refer to the green channel. Abbreviations: RGB, red green blue; ICDAS, International Caries Detection and Assessment System; E-D, Enamel-Dentine scale. GLCM, gray level co-occurrence matrix; NGTDM, neighbouring gray tone difference matrix; GLDM, gray level dependence matrix.

enhancement.[36] The GLCM texture appears to capture the relevant contributions of contrast at higher wavelengths in classifying caries by ICDAS. Similarly, the Small Area High Gray Level Emphasis (SAHGLE) feature extracted from red channel, is highly relevant in E-D classification, as it identifies smaller zones with higher intensity, which are an indication of greater caries depth (D2-D3 classes).

Significant contributions are found also in the green channel features, with particular regard to the GLCM Difference Entropy (a measure of the variability in neighborhood intensity differences), which is among the most important predictors in both ICDAS and E-D classification. The higher the Entropy the higher the probability of belonging to class 0 (i.e., non-depth and less extensive caries). The same applies also to blue channel features, where Difference Entropy inversely correlates with ICDAS classification. Furthermore, in the blue channel, Maximum Probability also positively correlates with caries depth, determining E-D classification. Therefore, the more pairs of adjacent intensity values there are in the carious region, the greater the depth of the caries will be, as the prediction goes toward class 1. Clinically, blue lights are used to induce fluorescence to identify demineralized areas associated with carious lesions, relying on the different fluorescent properties of healthy and carious dental tissues when exposed to blue light, typically around 415 nm. Therefore, there is also clinical support for these findings. The RGB channels' analysis highlights first-order statistical features where the green channel's median intensity predicts less severe caries (ICDAS class 0), and the red channel's maximum intensity suggests deeper caries (E-D), aligning with clinical observations using near-infrared transillumination, in which decayed transilluminated teeth appear darker than healthy tissue.[37] From the curves of the reverse cumulative distribution of residuals, shown in Fig. 5, it emerges that for both the ICDAS and E-D classification the minor residuals in most cases are obtained using the green channel and the RGB features, therefore in these cases, there are predictions closer to the real values.

Then, considering the RGB case, a case-wise analysis was done to evaluate the local explanations of the individual observations. Observations of case 0 and case 1 were considered for ICDAS and E-D, and the Break Down profiles were evaluated as shown in Fig. 6.

Looking at the local explanations for ICDAS classification, for the class 0 observation what has already been seen with the PDPs is confirmed, i.e. the negative prediction is more influenced by the median of the intensity values of the green channel and by the skewness of the intensity values on the red channel.

For class 1 observation, however, the texture features on the red channel are more impactful, the Cluster

Prominence which is a measure of the skewness and asymmetry of the GLCM, and the contrast in the NGTDM class, which is a measure of spatial intensity change, also dependent on the overall intensity level dynamic range.

Looking at the local explanations for E-D classification, for class 0 the negative prediction is more influenced by the median of the intensity values of the green channel, as for the ICDAS classification. For class 1 observation what has already been seen with the PDPs is confirmed, i.e. the positive prediction is more influenced by the maximum of the intensity values of the red channel.

Although this study provides new insights by using a radiomics approach for detecting caries in intraoral photographs, it does have some constraints. The quality and consistency of intraoral photographs can vary significantly, which might affect the model's accuracy. Standardizing imaging protocols could enhance reliability. In this study, we aimed to evaluate the performance of 150 dpi resolution images. Future research may explore the impact of higher-resolution images, carefully assessing their performance relative to increased data volume and computational demands. In addition, integrating radiomic approach into routine clinical practice requires not only technological adaptation but also training on larger and multicenter datasets. A validation on an external dataset is also necessary, but no available dataset, to our knowledge, presents a segmentation and labeling of lesions according to E-D scale.

This study validates a radiomics approach using intraoral images to classify dental caries depth and extent, achieving up to 94% accuracy. Texture features, especially from the green and red channels, strongly influence predictions, while the blue channel has less impact. Key features affecting ICDAS values include contrast in the red channel and difference entropy in the green and blue channels, reflecting non-homogeneous lesions with dark shadows. For E-D classification, high gray level emphasis in the red channel and entropy-related features in green and blue channels correlate with lesion severity. Integrating RGB channels reduces residual errors, improving diagnostic accuracy. This innovative method allows the use of relatively inexpensive and less invasive equipment, making it highly suitable for wide application.

Declaration of competing interest

The authors declare that they have no conflict of interests.

Acknowledgments

This research work has been conducted in collaboration with Maipek s.r.l. (Naples, Italy). Special thanks to Raffaele Pelliccio at Maipek for supporting the study.

Appendix A. Supplementary data

Supplementary data to this article can be found online at https://doi.org/10.1016/j.jds.2025.04.006.

References

1. Patcas R, Bernini DAJ, Volokitin A, Agustsson E, Rothe R, Timofte R. Applying artificial intelligence to assess the impact of orthognathic treatment on facial attractiveness and estimated age. *Int J Oral Maxillofac Surg* 2019;48:77—83.
2. Revilla-León M, Gómez-Polo M, Barmak AB, et al. Artificial intelligence models for diagnosing gingivitis and periodontal disease: a systematic review. *J Prosthet Dent* 2023;130:816—24.
3. Bassani S, Santonicco N, Eccher A, et al. Artificial intelligence in head and neck cancer diagnosis. *J Pathol Inf* 2022;13:100153.
4. Soltani P, Devlin H, Etemadi Sh M, Rengo C, Spagnuolo G, Baghaei K. Do metal artifact reduction algorithms influence the detection of implant-related injuries to the inferior alveolar canal in CBCT images? *BMC Oral Health* 2024;24:268.
5. Mohammad-Rahimi H, Motamedian SR, Rohban MH, et al. Deep learning for caries detection: a systematic review. *J Dent* 2022;122:104115.
6. Ammar N, Kühnisch J. Diagnostic performance of artificial intelligence-aided caries detection on bitewing radiographs: a systematic review and meta-analysis. *Jpn Dent Sci Rev* 2024;60:128—36.
7. Kühnisch J, Meyer O, Hesenius M, Hickel R, Gruhn V. Caries detection on intraoral images using artificial intelligence. *J Dent Res* 2022;101:158—65.
8. Moharrami M, Farmer J, Singhal S, et al. Detecting dental caries on oral photographs using artificial intelligence: a systematic review. *Oral Dis* 2024;30:1765—83.
9. Ponsiglione AM, Angelone F, Amato F, Sansone M. A statistical approach to assess the Robustness of radiomics features in the discrimination of mammographic lesions. *J Personalized Med* 2023;13:1104.
10. Angelone F, Ciliberti FK, Tobia GP, et al. Knee cartilage degradation in the medial and lateral anatomical compartments: a radiomics study. In: *2024 IEEE international conference on metrology for eXtended reality, artificial intelligence and neural engineering (MetroXRAINE)*; 2024:183—8.
11. Angelone F, Ponsiglione AM, Ricciardi C, et al. A machine learning approach for breast cancer risk prediction in digital mammography. *Appl Sci* 2024;14:10315.
12. Orlhac F, Nioche C, Klyuzhin I, Rahmim A, Buvat I. Radiomics in PET imaging: a practical guide for newcomers. *Pet Clin* 2021;16:597—612.
13. Schick U, Lucia F, Dissaux G, et al. MRI-derived radiomics: methodology and clinical applications in the field of pelvic oncology. *Br J Radiol* 2019;92:20190105.
14. Aerts HJ, Velazquez ER, Leijenaar RT, et al. Decoding tumour phenotype by noninvasive imaging using a quantitative radiomics approach. *Nat Commun* 2024;5:4006.
15. Angelone F, Ponsiglione AM, Belfiore MP, et al. Evaluation of breast density variability between right and left breasts. In: *Atti del Convegno Nazionale di Bioingegneria*. Patron Editore Srl, 2023.
16. Gillies RJ, Kinahan PE, Hricak H. Radiomics: images are more than pictures, they are data. *Radiology* 2016;278:563—77.
17. Cantu AG, Carrillo-Perez F, Morales JO, Vargas L. AI-powered caries detection: analysis of oral photographs for early diagnosis. *J Dent Res* 2020;99:123—30.
18. Khan H, Rehman A, Ali S, et al. Deep learning approaches for caries detection using oral images: a review. *Front Dent AI* 2021;2:95—103.
19. Lee JH, Kim DH, Jeong SN, Choi SH. Diagnosis and prediction of periodontally compromised teeth using a deep learning-based convolutional neural network algorithm. *J Periodontal Implant Sci* 2018;48:114—23.

20. Angelone F, Ponsiglione AM, Ricciardi C, Cesarelli G, Sansone M, Amato F. Diagnostic applications of intraoral scanners: a systematic review. *J Imaging* 2023;9:134.
21. Russell BC, Torralba A, Murphy KP, Freeman WT. LabelMe: a database and web-based tool for image annotation. *Int J Comput Vis* 2008;77:157—73.
22. Gugnani N, Pandit I, Srivastava N, Gupta M, Sharma M. International Caries Detection and Assessment System (ICDAS): a new concept. *Int J Clin Pediatr Dent* 2011;4:93—100.
23. Van Griethuysen JJ, Fedorov A, Parmar C, et al. Computational radiomics system to decode the radiographic phenotype. *Cancer Res* 2017;77:e104—7.
24. Zwanenburg A, Vallières M, Abdalah MA, et al. The image biomarker standardization initiative: standardized quantitative radiomics for high-throughput image-based phenotyping. *Radiology* 2020;295:328—38.
25. Demircioğlu A. Measuring the bias of incorrect application of feature selection when using cross-validation in radiomics. *Insights Imaging* 2021;12:172.
26. Heckman JJ. Sample selection bias as a specification error. *Econometrica* 1979;47:153—61.
27. Kuhn M, Johnson K. *Applied predictive modeling*. New York, NY: Springer, 2013.
28. Wang R, Tang K. Feature selection for maximizing the area under the ROC curve. In: *2009 IEEE international conference on data mining workshops*; 2009:400—5.
29. Urbanowicz RJ, Meeker M, La Cava W, Olson RS, Moore JH. Relief-based feature selection: introduction and review. *J Biomed Informatics* 2018;85:189—203.
30. Muthukrishnan R, Rohini R. LASSO: a feature selection technique in predictive modeling for machine learning. In: *2016 IEEE international conference on advances in computer applications (ICACA)*; 2016:18—20.
31. Kuhn M. Building predictive models in R using the caret package. *J Stat Software* 2008;28:1—26.
32. Saranya A, Subhashini R. A systematic review of explainable artificial intelligence models and applications: recent developments and future trends. *Decis Anal J* 2023;7:100230.
33. Friedman JH. Greedy function approximation: a gradient boosting machine. *Ann Stat* 2001;29:1189—232.
34. Biecek P, Burzykowski T. *Explanatory model analysis: explore, explain, and examine predictive models*. New York: Chapman and Hall/CRC, 2021.
35. Biecek P. DALEX: explainers for complex predictive models in R. *J Mach Learn Res* 2018;19:1—5.
36. Ortiz MIG, de Melo Alencar C, De Paula BLF, Magno MB, Maia LC, Silva CM. Accuracy of near-infrared light transillumination (NILT) compared to bitewing radiograph for detection of interproximal caries in the permanent dentition: a systematic review and meta-analysis. *J Dent* 2020;98:103351.
37. Michou S, Lambach MS, Ntovas P, et al. Automated caries detection in vivo using a 3D intraoral scanner. *Sci Rep* 2021;11:21276.